ON THE SEARCH FOR NEAR-EARTH ASTEROIDS

JACK DRUMMOND and DAVID RABINOWITZ
University of Arizona

and

MARTIN HOFFMANN
Observatorium Hoher List der Universitäts-Sternwarte Bonn

The distribution of known asteroids in Earth-approaching orbits is a biased sample, but does lead to predictions where objects may be found. To date, searches for near-Earth asteroids have concentrated on the opposition direction, but it is obvious that as systems push to fainter limiting magnitudes more asteroids will be discovered closer to the Sun. These will include Earth-approaching asteroids observed away from the Earth and objects interior to the orbit of the Earth that will never pass through opposition. Least-squares fits to the density distribution of known near-Earth asteroids are presented as preliminary functions to be debiased in order to obtain a true distribution. Some of the biases are reviewed. It appears, especially if searches are made closer to the Sun, that with some reasonable assumptions, the biases that exist may be described, leading to a better understanding of the dynamics that result in the observed distribution of Earth-approaching asteroids. CCDs promise to supplant photography as the preferred search method.

Until recently, near-Earth asteroids (NEAs) were only discovered accidentally, but as programs deliberately designed to detect close asteroids have reached full operational capability the number discovered has increased dramatically. Although of immense popular appeal because of their inferred apocalyptical portent, the NEAs are also of interest to astronomers and meteoriticists, for they are the smallest asteroids that can be studied from the Earth and have a direct relation to the meteorites available for laboratory study. Furthermore, among the Earth-approaching asteroids are extinct or dormant comets, missing links that could elucidate the relationship between asteroids and comets. As potential resources for human exploitation, NEAs to date remain largely terra incognita. Therefore, both quantitatively and qualitatively, that is, in their numbers and in specific cases, near-Earth asteroids deserve special study and specialized searches.

In this chapter, we do not recount the detailed history of NEA searches, but instead concentrate on the distribution and biases of observed NEAs. In the first section, we develop a detailed distribution density function describing where in the sky NEAs can be found from a geocentric point of view, based on the known, not extrapolated, population, and comment on its implication

for searches. Next (Sec. II), we discuss some of the biases that exist in this observationally determined set of NEAs. A brief outline of the future direction of NEA searches with CCDs is presented in Sec. III, followed by some conclusions on the topics in Sec. IV.

I. ORBIT DISTRIBUTIONS

There are two approaches to searching for the generally small ($\sim$1 km) asteroids that glide swiftly by the Earth. The first, and most commonly used, is to search around the opposition point where the asteroids will be near a minimum in phase angle, and therefore the brightest, and will be moving the fastest, more than a degree per day. Even slow, distant objects are brightest and moving fastest near their opposition. The second, and to date untried, approach, is to search the apex and antapex of the Earth's way, tangent to the Earth's orbit, where the asteroids that will be overtaken by the Earth or will overtake the Earth, respectively, can be seen moving the slowest. A third method, introduced here in the last paragraph of this section, is to search a particular volume of space from anywhere in the Earth's orbit.

To illustrate the distribution of NEAs, and where to search for them, Figs. 1–8 are provided. First, Fig. 1 shows the distribution of orbital elements, compared two at a time, for all 157 numbered and unnumbered asteroids (supplied by J. Scotti) with perihelion distances $<$1.3 AU (the working definition for NEAs) through the end of 1990 and the three meteorites with known orbits calculated from multiply photographed falls. The strongest correlation (r^2 = 0.21) appears between q and e. This is partly an observational bias, but partly reflects a real correlation in the distribution. It is doubtful, for instance, that there are as many low-eccentricity asteroids near Mercury or Venus as there are near the Earth because of dynamical considerations, and the low e, low q region in Fig. 1 would remain depleted even if the observed distribution were debiased.

The lower three panels in Fig. 1, where the orientation of the orbits are compared to q, e and i, illustrate no real correlation. Figure 2, then, can be produced to indicate the observational distribution of NEAs. Choosing a night at random (April 4), 360 1-km diameter S asteroids, with albedos of 0.186 (Tedesco et al. 1989), H = 17.5, were placed in every orbit at one degree intervals of mean anomaly, and the apparent magnitudes calculated using a Lumme and Bowell phase slope of 0.23 (Lagerkvist and Magnusson 1990). Figures 2a, 2b and 2c show the positions of the asteroids to limiting magnitudes of 15, 17.5 and 20, respectively, in ecliptic coordinates centered on the opposition point. Alternatively, Fig. 2 can be viewed as representing a range in sizes of objects. If the middle panel represents 1-km objects at apparent magnitude 17.5 and brighter, then 2a and 2c show objects $\sqrt{10}$ times smaller and larger, respectively. Some interesting considerations become apparent from Fig. 2. First note that for bright limiting magnitudes or for smaller objects (Fig. 2a), the best place to search is over all the sky centered

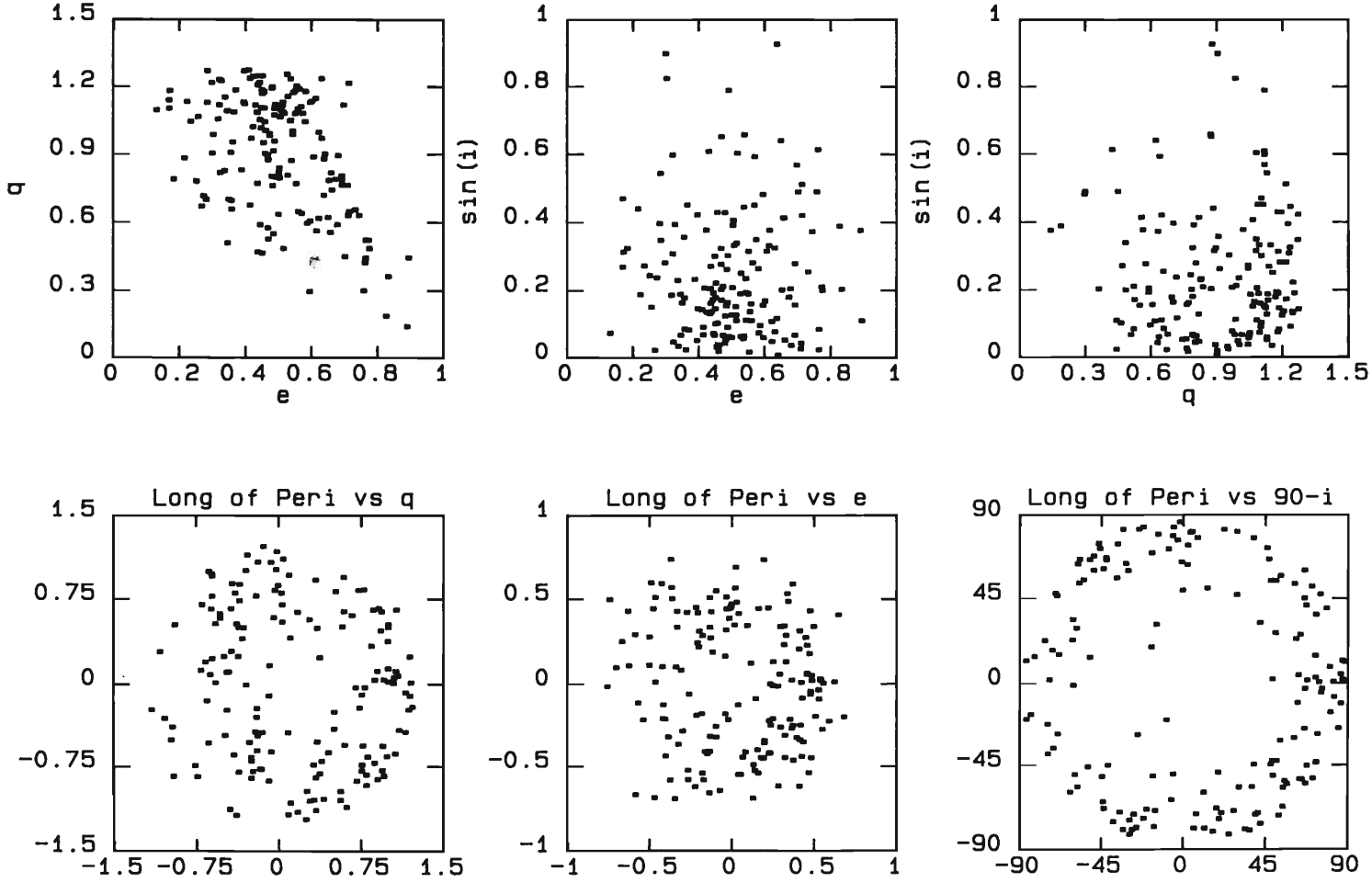

Figure 1. The distribution of orbital elements of 157 NEAs and three meteorites with known orbits. Pairs of orbital elements (or functions of elements) are compared two at a time. For the bottom panel involving the longitude of perihelion, the longitude is measured counterclockwise from the right, while the other parameter is measured from the center outward according to the scale (figure from Drummond 1991, but extended through 1990XJ).

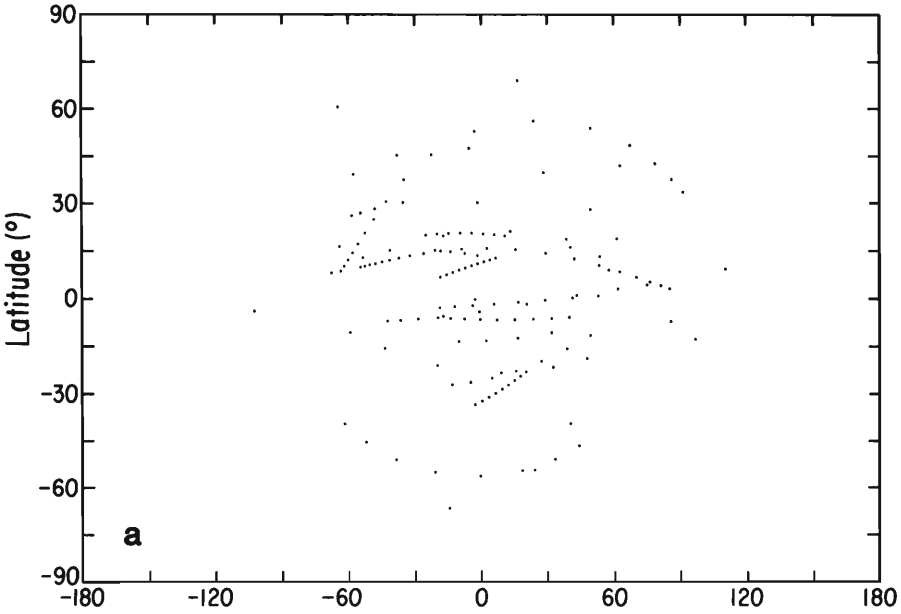
90
60
30
0
-30
-60
-90
Latitude (°)
a
-180
-120
-60
0
60
120
180

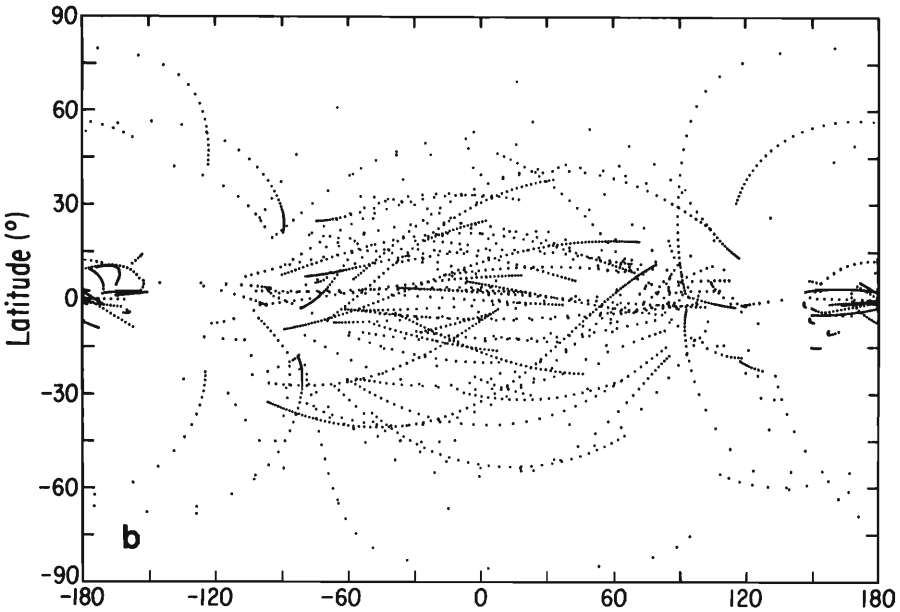
90
60
30
0
-30
-60
-90
Latitude (°)
b
-180
-120
-60
0
60
120
180

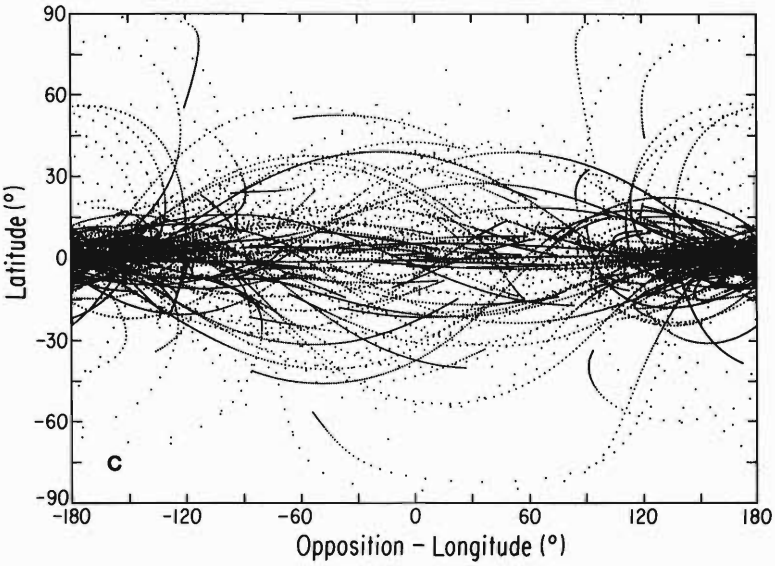

Figure 2. The distribution of NEAs on a random night, plotted in ecliptic coordinates with respect to the longitude of the opposition point (evening is to the right, morning to the left). 360 1-km S asteroids are placed in the 160 orbits of known objects at one degree intervals of mean anomaly (thus taking into account dwell time), and those brighter than apparent V magnitude 15 (panel a), 17.5 (panel b) and 20 (panel c), are plotted. Note that a system with a bright limiting magnitude detects 1 km objects in the known orbits only within 90° of the opposition point, whereas 1 km objects can be detected almost anywhere along the ecliptic, and especially near the Sun, by a system with a limiting magnitude of 20. Alternatively, for a fixed limiting magnitude of 17.5, the three panels, a, b and c, show an upper diameter limit of 0.32, 1 and 3.2 km. Thus a system with a limiting magnitude of 17.5 would detect 3.2 km objects all along the ecliptic, with increased concentrations near the Sun (panel c). As another example, for a system with a limiting magnitude of 22.5, panels a to c show the positions of asteroids in known orbits smaller than diameters of 32, 100 and 320 m.

on the opposition direction. However, for larger asteroids or for systems with faint limiting magnitudes (Fig. 2c), the best place to search (except for one glaring problem) would be around the Sun where many asteroids are at superior conjunction and bright because of a minimum in phase angle. The intermediate case (Fig. 2b) is the most instructive, for it shows where not to look for asteroids. A definite minimum in concentration occurs at 45° from the Sun, where the phase angles and distances conspire to render asteroids faint in these parts of their orbits. Nevertheless, even in Fig. 2b a concentration near the Sun can be seen. Around opposition, away from the Sun, and scattered all over the sky, but not particularly concentrated toward the ecliptic, are the asteroids that are passing through perihelion just outside the orbit of the Earth. The apex and antapex of the Earth's way appear as radiants for many of the orbits, causing a slight but noticeable increase in the density of points 90° from the Sun in Fig. 2b.

Figure 3a shows the probability density P for all 57,600 points in the 160 orbits, (360 points per orbit), in 3600 equal-area cells of 0.2 square degrees, and Fig. 3b shows a least-squares fit using the first few relevant terms in a spherical harmonic expansion according to

$$P = \exp\{a_0 + a_1 \cos(\lambda)\cos(\beta) + a_2[\cos(\lambda)\cos(\beta)]^2 + a_3 \cos^2(\beta)\} \quad (1)$$

where λ and β are the ecliptic longitude of the opposition point minus longitude of the asteroid, and the ecliptic latitude for each point, respectively, and

$$a_0 = -15.162,\ a_1 = -0.7288,\ a_2 = .06852,\ a_3 = 9.6818. \quad (2)$$

Such a fit describes the probability of finding an orbit point in a cell to no worse than 0.3% of the total observed distribution, with a standard error over all the sky 10 times smaller.

Taking the brightness of the asteroids into consideration, a probability distribution can be formulated as a function of magnitude V as well as position with respect to the opposition point. Qualitatively, the brightest 2% of the asteroids (brighter than $V = 17.5$ for 1 km objects, brighter than 22.5 for 100 m objects, etc.) can be found centered around the opposition point. There is an abrupt transition at this magnitude, where most of the remaining objects can be found centered on the Sun. The following mathematical probability distribution performs poorly in accounting for this transition, but does well for the brightest 2% and the faintest 50% of the observed orbit points. Even in the worst case in the transition from opposition to Sun-centered objects, the deviation between the model and the observed distribution is 0.8%, and overall the model describes the probabilty of finding a 1 km object at a given position and magnitude to within a standard error of 0.04%. This probability per square degree per magnitude for 1 km S objects is given by

$$P = \exp\{a_0 + a_1 \cos(\lambda)\cos(\beta) + a_2[\cos(\lambda)\cos(\beta)]^2 +$$

$$a_3 \cos^2(\beta) + a_4 V + a_5 V^2 + a_6 V \cos(\lambda)\cos(\beta)\} \quad (3)$$

where $a_0 = -44.132$, $a_1 = 1.900$, $a_2 = -0.319$, $a_3 = 3.950$, $a_4 = 3.176$, $a_5 = -0.0772$, $a_6 = -0.0977$. For a given size distribution, it is only necessary to integrate Eq. (2) and multiply by a size distribution function to obtain the total probability for finding objects in a given magnitude and size range for a given area of the sky.

If the heliocentric XYZ coordinates of all 57,600 points are converted to $R\theta$ coordinates, thus putting every point on the meridian from the Earth's point of view, the distribution of orbit points within 0.5 AU of the Earth's orbit is shown in Fig. 4a, the distribution in the RZ plane. The resulting probability distribution is shown in cells of 0.015625 square AUs in Fig. 4b. R is the distance from the Sun to the projection of the point onto the ecliptic plane

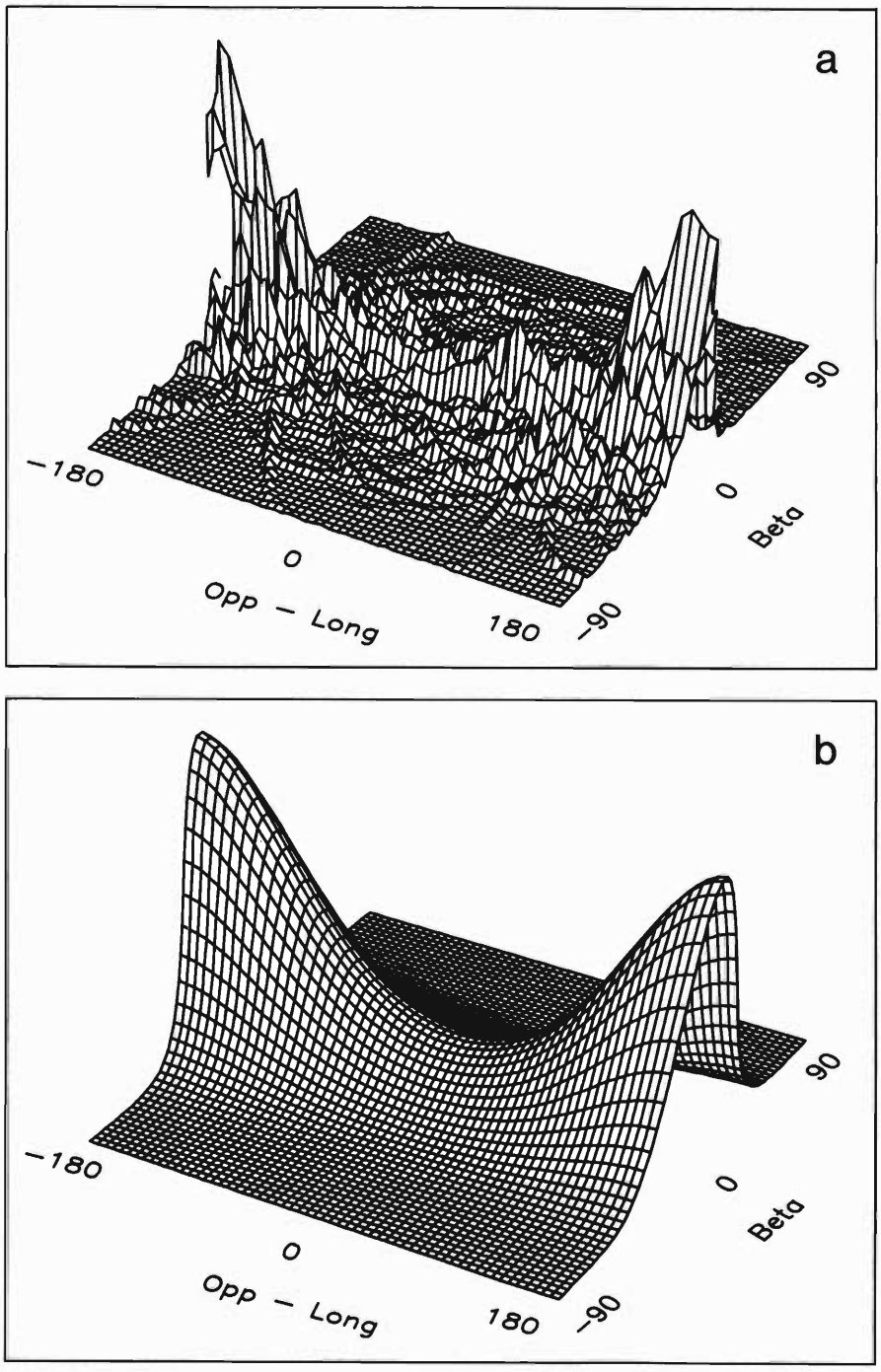

Figure 3. (a) The probability or density distribution of all 57600 orbit points (160×360) of known orbits of NEAs and (three) meteorites, plotted as in Fig. 2, but in equal area cells of 0.2 square degrees. (b) The theoretical distribution according to Eq. (1).

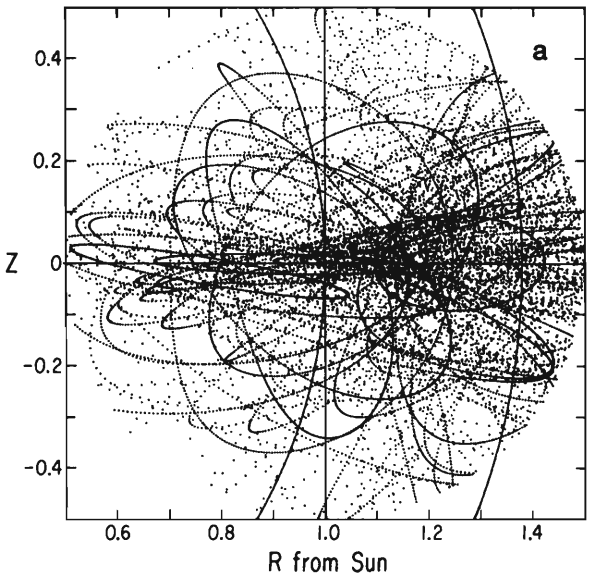
a
0.4
0.2
Z 0
-0.2
-0.4
0.6
0.8
1.0
1.2
1.4
R from Sun

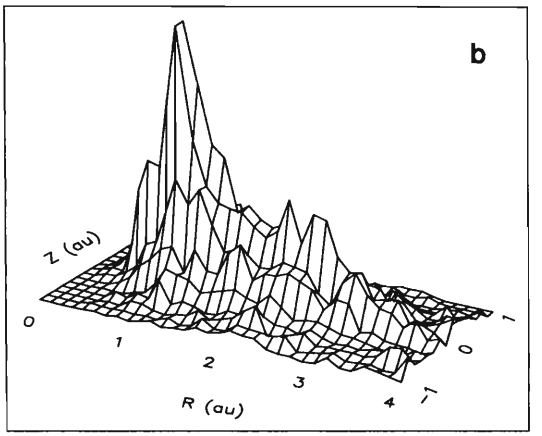
b
Z (au)
0
1
2
3
4
R (au)
1
0
-1

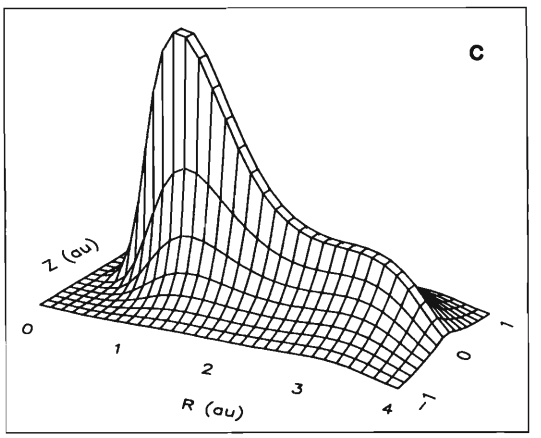
c
Z (au)
0
1
2
3
4
R (au)
1
0
-1

($R^2 = X^2 + Y^2$) and θ is the heliocentric ecliptic latitude [$\theta = \arctan(Z/R)$]. Figure 4c shows the least-squares fit according to

$$P = \exp[a_0 + a_1|\theta| + a_2 R_\odot + a_3 R_\odot^2 + a_4 R_\odot^3 + a_5 R_\odot^4] \qquad (4)$$

where P is the probability per AU^2, $R_\odot^2 = X^2 + Y^2 + Z^2$ is the heliocentric distance squared, and $a_0 = -7.068$, $a_1 = -6.421$, $a_2 = 16.184$, $a_3 = -12.420$, $a_4 = 3.776$, $a_5 = -0.4049$. The worst deviation is 0.6% and the standard error is 20 times smaller. This probability distribution and Eqs. (1) and (2) are the functions which must be debiased to extract the true distributions of the NEA population. Figure 4, for instance, shows that the observed probability peaks strongly just outside the orbit of the Earth, between 1.125 and 1.25 AU, and within 0.0625 AU of the ecliptic plane. Orbits that pass through this region stand the greatest possibility of being discovered. (For information on debiased population estimates see Shoemaker et al. [1990] and the Chapter by Davis et al.)

Another illustration of the visibility of NEAs is given in Fig. 5, where asteroids are distributed at random in orbits of real NEAs and main-belt asteroids (but with randomized arguments of perihelion and longitudes of ascending node) and according to a distribution of sizes e^H, where H is the absolute magnitude. The range of H for main-belt objects is 3 to 23 and for NEAs 10 to 30; only objects appearing brighter than visual magnitude 20.5 (using a phase function of 0.1) are plotted. The probability function for the NEA component of this distribution should correspond to the function that would be obtained by multiplying Eq. (2) by e^H and integrating from $V = -\infty$ to 20.5 and from $H = 10$ to 30. Notice that the background of main-belt asteroids concentrate toward the opposition point, while the NEAs scatter more evenly about the sky.

Rates of apparent motion can be used to discriminate NEAs from main-

Figure 4. The probability or density distribution of the 57,600 orbit points within 0.5 AU of the Earth, plotted in RZ coordinates. (a) All of the individual orbit points are plotted, with positive Z being above the ecliptic plane. Note the concentration of dots between 1 and 1.2 AU, in and just above the ecliptic plane, indicating that most orbits pass through this region or, much more likely, that there is a discovery bias favoring objects that pass through this region. The two curved lines through the field are at distances of 1 and 1.38 AU from the Sun (the perihelion distance of Mars). (b) The relative density of points in cells of 0.015625 AU^2. Again note the concentration of points near 1 AU in the Ecliptic plane, but also the presence of secondary peaks in the asteroid belt between 2 and 3 AU. (c) The theoretical distribution according to Eq. (3).

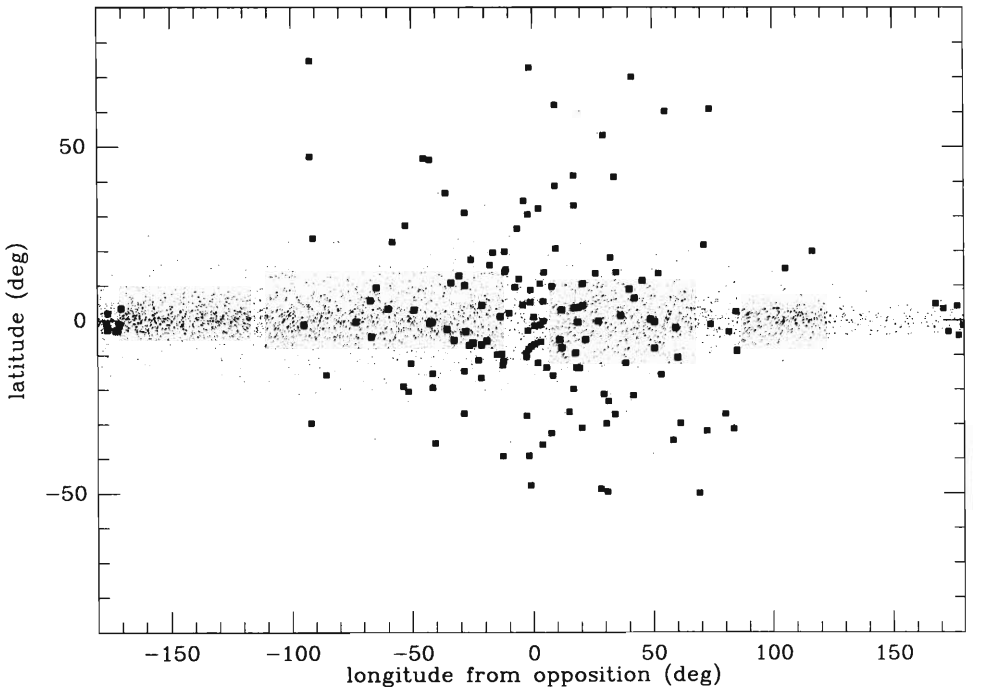

Figure 5. The distribution of NEA (boxes) and main-belt (dots) asteroids according to the theoretical size distribution given in the text.

belt objects. Retrograde NEAs moving faster than $>0\overset{\circ}{.}5$ day^{-1} at opposition are easily distinguished by their greater rates of motion. All prograde asteroids are identified as NEAs. Figure 6a shows the rates less than $0\overset{\circ}{.}5$ day^{-1} near opposition for a simulated population of asteroids such as is shown in Fig. 5, and illustrates that the slowly moving NEAs can be distinguished by their direction of motion. Figure 6b shows angular rates at opposition vs apparent magnitude for a simulated population of NEAs only. It is apparent that a system which can identify slowly moving ($<0\overset{\circ}{.}5$ day^{-1}) NEAs fainter than 17th magnitude by their direction of motion also samples the densest area of the distribution, and will identify the greatest number. These conclusions are being verified by the Spacewatch Telescope, which is finding slow, large NEAs farther than 1 AU from the Earth.

Rather than search in the opposition direction, or in the direction of the apex and antapex of the Earth's way, a third way is to conduct searches along specific orbits. The four asteroid/fireball streams of Drummond (1991) and Halliday et al. (1990) lend themselves to a search of a fixed volume in space throughout the year. (In an updated analysis, 1991FA has been added to the third stream, bringing to five the number of asteroids in each of the first three streams.) The bottlenecks that occur near perihelion in the orbits of the individual members are about 0.1 AU in diameter for the asteroids of the first three streams, and occur when the asteroids are traveling at 35 km s^{-1}. (The

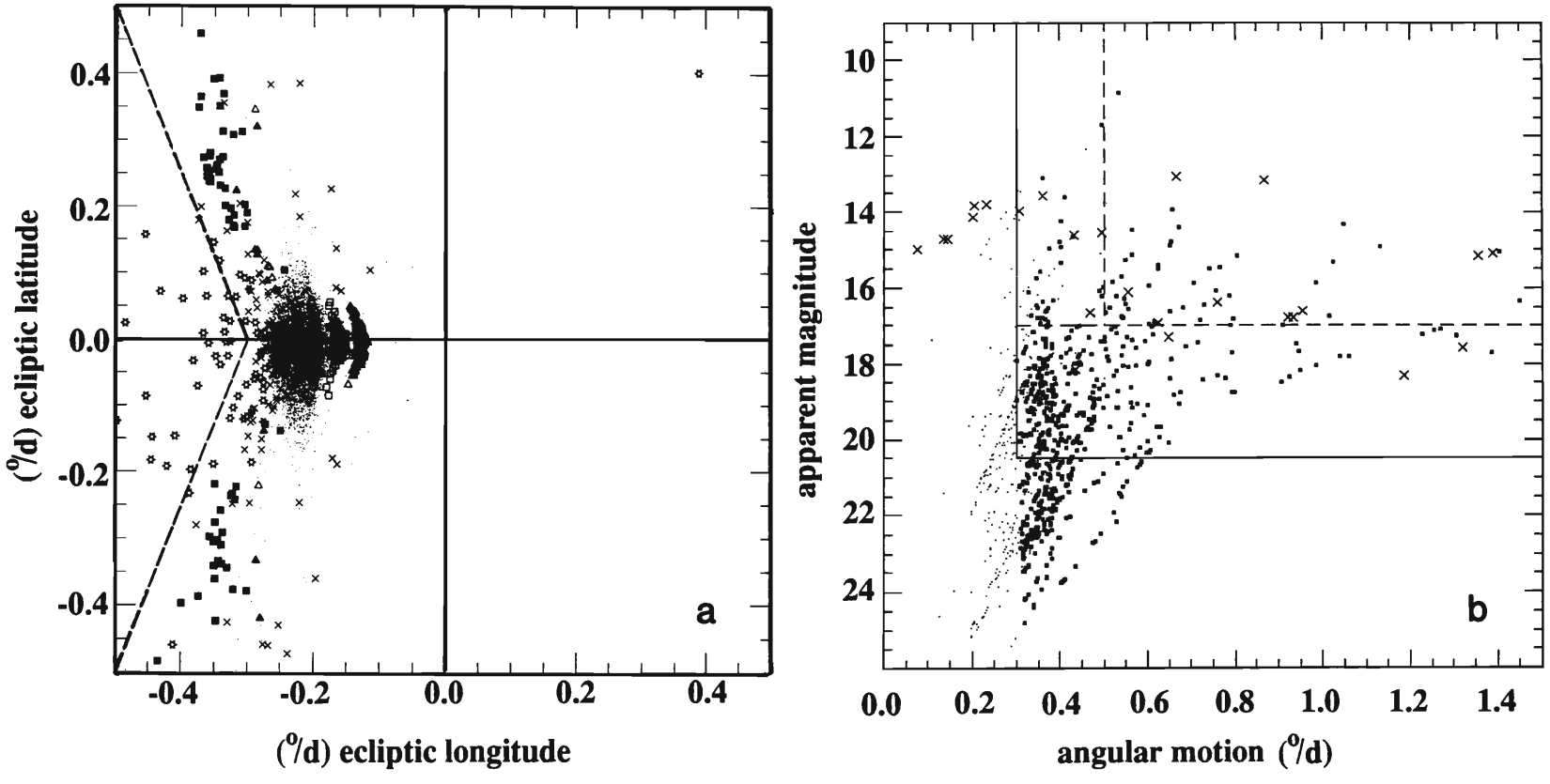

Figure 6. (a) Rates of motion for the theoretical NEA population shown in Fig. 5 and discussed in the text. Also shown are the expected rates for other asteroid types. Many NEAs move faster than 0°.5 per day, but the figure only covers slower rates. NEAs are depicted with open stars and are the only objects to the left of the dashed line, indicating that they can be uniquely identified by their direction of motion. Other kinds of asteroids depicted are Main Belt (dots), Trojans (open triangles), Phocaeas (solid triangles), Hildas (open squares), Hungarias (solid squares) and Mars crossers (X). (b) Apparent magnitude vs rates of motion for a theoretical distribution of NEAs only. Solid squares (prograde) and Xs (retrograde) show NEAs that can be identified strictly by their motions (from Rabinowitz 1991).

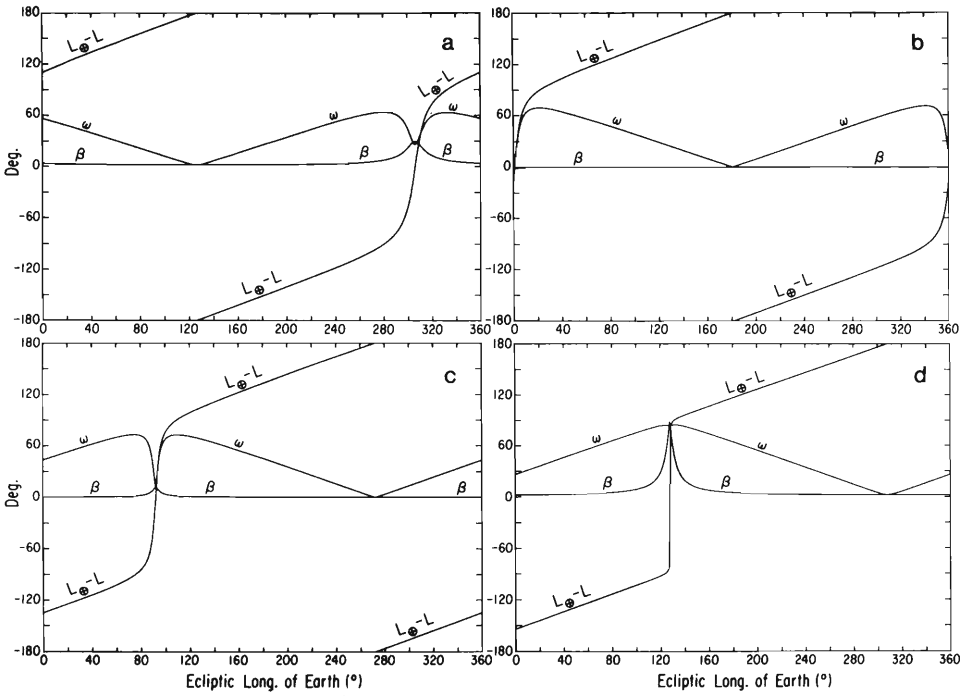

Figure 7. Observability of four (a–d) asteroid stream bottlenecks. Each panel shows three continuous curves, ecliptic longitude with respect to the opposition point ($L_\oplus - L$), ecliptic latitude (β), and solar phase angle (ω) throughout the year (ecliptic longitude of Earth). For example, the scrunch point for Association I (plot a) reaches a maximum in latitude ($\beta = 29°$) on July 29 (Ecl. Long. of Earth = 306°), when it is at opposition ($L_\oplus - L = 0°$), and the phase angle reaches a secondary minumum of 29°. Most of the year the scrunch point is at very low latitudes. The phase angle's deepest minimun occurs when the scrunch point is behind the Sun. The three associations are the asteroid streams of Drummond (1991), while the fourth is for a stream defined by five fireballs (Halliday et al. 1990) and 1989DA; the observability parameters are calculated assuming the characteristics of the three other asteroid streams and applying them to the orbit of 1989DA.

fourth stream, which is comprised of five fireballs and one asteroid, 1989DA, is given the same parameters centered on the orbit of the asteroid.) The density of the stream is maximum here, where the individual orbits pinch together and the flux through the volume is greatest, presenting the best opportunity for the discovery of new members. Figure 7 shows the ecliptic coordinates with respect to the opposition point for the fixed scrunch points or regions during the course of the year. Note that the scrunch point is generally very near the ecliptic, only changing in latitude as it approaches opposition. For objects passing through this volume, the solar phase angle shown on the same plot reaches two minima, with the lowest usually occurring when the scrunch point is at superior conjunction. In Fig. 8, the apparent diameter of the fixed volume is generally around 4° for most of the year, but shoots up to 40° at opposition for Stream I, and up to 88° for Stream III. The apparent

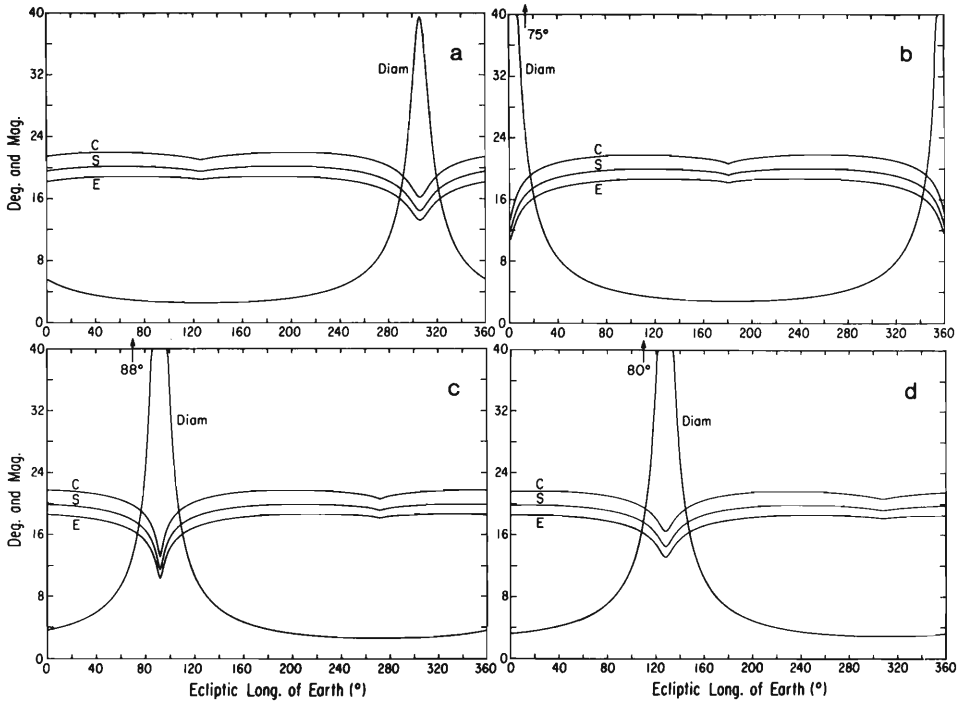

Figure 8. Apparent size of each (a–d) scrunch region and magnitude of a 1-km object passing through it. Throughout the year the 0.1 AU diameter of the bottlenecks have an apparent diameter of 4°, but can shoot up to more than 80° when the Earth is close to the scrunch point. The apparent magnitudes of a 1-km C, S and M asteroid are generally around magnitude 20 throughout the year.

magnitudes of a 1-km C, S and E object are shown to be rather steady until a month or two around opposition. This suggests that systems with bright limiting magnitudes but large fields of view should search for new members passing through the bottleneck at opposition, while systems with small fields of view but faint limiting magnitudes should follow the scrunch regions at other times of the year. The rates of motion for objects passing through all three regions is always greater than 1° per day, regardless of when the area is searched, allowing them to be distinguished from main-belt asteroids.

II. NEA BIASES

Both their accessiblity (represented by the distribution of orbital elements) and their composition (determined by the distribution of their sources—comets or asteroids) are important if NEAs are to be understood as carriers of resources. The result of the previous section, where the distribution of asteroids follows from the biased distribution of their detection location, allows for many possible true distributions of orbital elements. Even simple observational preferences and biases can skew any of several theoretical asteroid distributions to produce the observed distribution. Furthermore, the small

number of searches at small elongations from the Sun leave a considerable volume of space and orbital phase largely unexplored. On the other hand, a consideration of the efficiencies of the sources and sinks of NEAs, and of physical parameters and processes involved, does provide some constraints on the search for and detection of NEAs.

Today's distribution of NEAs is a composite distribution with varied origins. Aside from possible, but as yet undetected, fossil asteroids left over from the creation of the inner solar system (vulcanoids—planetesimals interior to Mercury, and Trojans of Mercury, Venus and Earth), the fraction of NEAs of cometary or asteroid-belt origin remains uncertain. Both of these groups should be subdivided in considering orbital element distributions. Extinct comets can be de-coupled from Jupiter family orbits by multiple dynamical interactions with the terrestrial planets (Wetherill 1991) and by nongravitational forces. Even if comets cannot survive devolitization in the inner solar system without being turned to dust, they can survive as asteroid-like objects in the outer, less irradiated parts of the solar system. Such objects, as represented by Chiron, may dynamically evolve inward. Most NEAs arrive from the main belt by inward cascade through orbital resonances, passing through a Mars-crossing stage. Perhaps a few may begin the inward journey in a collision.

These different (cometary/main-belt) original groups differ primarily in their diameter frequencies (Hughes 1990; Gradie et al. 1989) and in their orbital eccentricities and inclinations. Their inward evolution does not change the slope of the diameter frequency of the objects but acts as a neutral filter for the number of a given diameter that penetrate certain dynamical regimes. Therefore, the diameter of the largest member, for instance, of the classical subgroups of inner solar system asteroids gradually decreases with decreasing mean heliocentric distance for the group. For Mars crossers, Amors, Apollos and Atens, the largest asteroids are, respectively, 313, 1036, 2212 and 2100, with diameters (Tedesco 1989) of 101, 41, 9 and 3 km.

Another characterization of different dynamical regimes is given by a modification of the classical Tisserand invariant, which is usually expressed in terms of the restricted three-body system Sun-Jupiter-object

$$T = a_J/a_A + 2\sqrt{a_A(1 - e_A^2)/a_J} \tag{5}$$

where a_J and a_A are the semimajor axes of Jupiter and an asteroid, and e_A is the eccentricity of the asteroid. Replacing Jupiter by any of the terrestrial planets, the Earth in this instance, a significant number of NEAs cluster close to $T = 3.0$, indicating its dominating influence, while objects with $T < 3.0$ have a more scattered distribution.

Because different groups of NEAs have different rates of motion and dwell times in the observability windows, the observational selection effects for the groups are quite complicated. Cases like 1685 Toro exist, whose 5:8 ratio of orbital period to the Earth's excludes close approaches over large

areas of the sky. Resonant coupling of some orbital elements is responsible for other kinds of avoidance of close approaches to the Earth by some NEAs.

Some asteroid/comet dichotomy is reflected in the dynamical classification of Milani et al. (1989), although the existence of several transition paths between the classes introduces ambiguities with respect to evolutionary interpretations. Fine structure in the original distribution of new or long-period comets, such as concentrations of perihelion directions (Fernandez and Ip 1991), become entirely averaged during the dynamical evolution into stabilized near-Earth objects. As so little is known about the possible ranges of mineralogies of residual cometary cores, or of asteroids, surface spectral characteristics cannot be safely used as a test of cometary vs asteroidal origin. Rotation frequencies of asteroid groups close to resonances in the main belt, where the path to the near-Earth environment begins, have not been studied sufficiently to compare with NEAs. The same holds true for asteroid shapes and pole orientations. However, such comparisons do provide hope that the transformation processes from main-belt to Earth-approaching objects may be understood in the future in such a way that links can be identified between well-defined subgroups in the main belt and the NEAs. Even in the biased distributions some significant fine structure can be recognized and should be taken into account when attempting to model the real distribution. NEA perihelia and aphelia close to the terrestrial planets are underabundant (Fig. 9). For Mars the zone of greatest depletion (Fig. 9b) is at its aphelion where a gap in asteroid aphelia occurs. The semimajor axes of mean motion resonances have a tendency to be overabundant for objects with higher eccentricties (Apollos), while for Amors the Kirkwood gaps at the 3:1 and 5:2 resonances are depleted.

Our knowledge of the distribution of orbital elements of NEAs is based on chance discoveries and systematic searches centered on the opposition point. Only one object has been found by groundbased observations at solar elongations less than 90° (Hahn 1988) and the mean elongation at the time of their discovery of all NEAs through February 1988 is 149°.4. Figure 10 shows the location and motion at the times of discoveries for all fast-moving objects discovered within 60° at opposition reported on the IAU Circulars from 1981 through mid 1991. Dominated by the Palomar Schmidt surveys of E. M. Shoemaker, C. S. Shoemaker and E. F. Helin, the distribution corresponds to Fig. 2 with a system limiting magnitude of 14.5 for 1-km-sized asteroids, or alternatively, using the estimated average 16.5 limiting magnitude for their system, Fig. 10 suggests that their program is discovering the 400 m objects and larger. The limiting magnitude of 20.5 for the Spacewatch Telescope software detection implies that it would discover primarily 60 m objects and larger.

However, two man-made factors contribute to the nonisotropy of detections. First, because all objects are brightest near the opposition point, most surveys follow the route to easiest detection and concentrate in this region. Second, the window of observability in dark time at low air mass is much

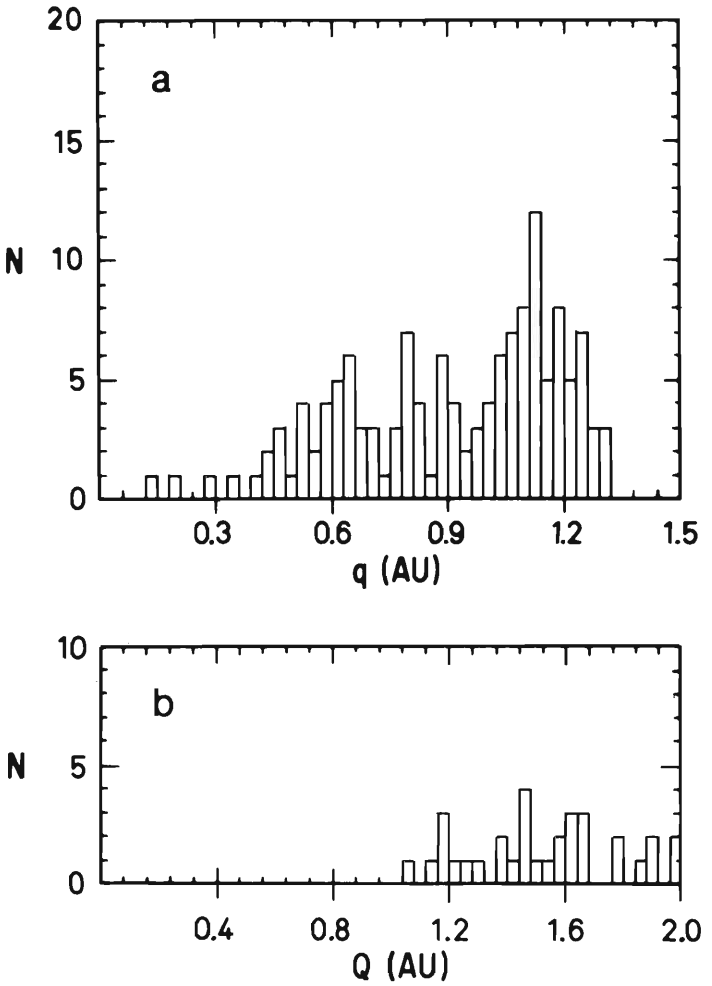

Figure 9. Histogram of NEA perihelion (a) and aphelion (b) distances. Note the gaps at the distances of the terrestrial planets: Mercury a = 0.39 AU, Venus 0.72, Earth 1.0, and near the aphelion distance of Mars at 1.67 (b).

smaller at low solar elongations. Furthermore, searches tend to concentrate towards the plane of the ecliptic and are influenced by the Milky Way. Because of such strong selection effects, the real distribution of NEAs may differ somewhat from the observed one. One way to model the selection effects is to assume an observing preference proportional to the $\sin l/2$, where l is the solar elongation. This accounts in a rough way for the observing time available at small solar elongations for observatories at intermediate latitudes. Another simple approach is to assume that all detections are made between fixed distances from the Sun, which is the case for a given observing station and a limiting size/magnitude, and then calculate the dwell time in this increment for various a's and e's. Table I gives such dwell times in fractions of orbital period for objects between 1 and 1.2 AU from the Sun. But even

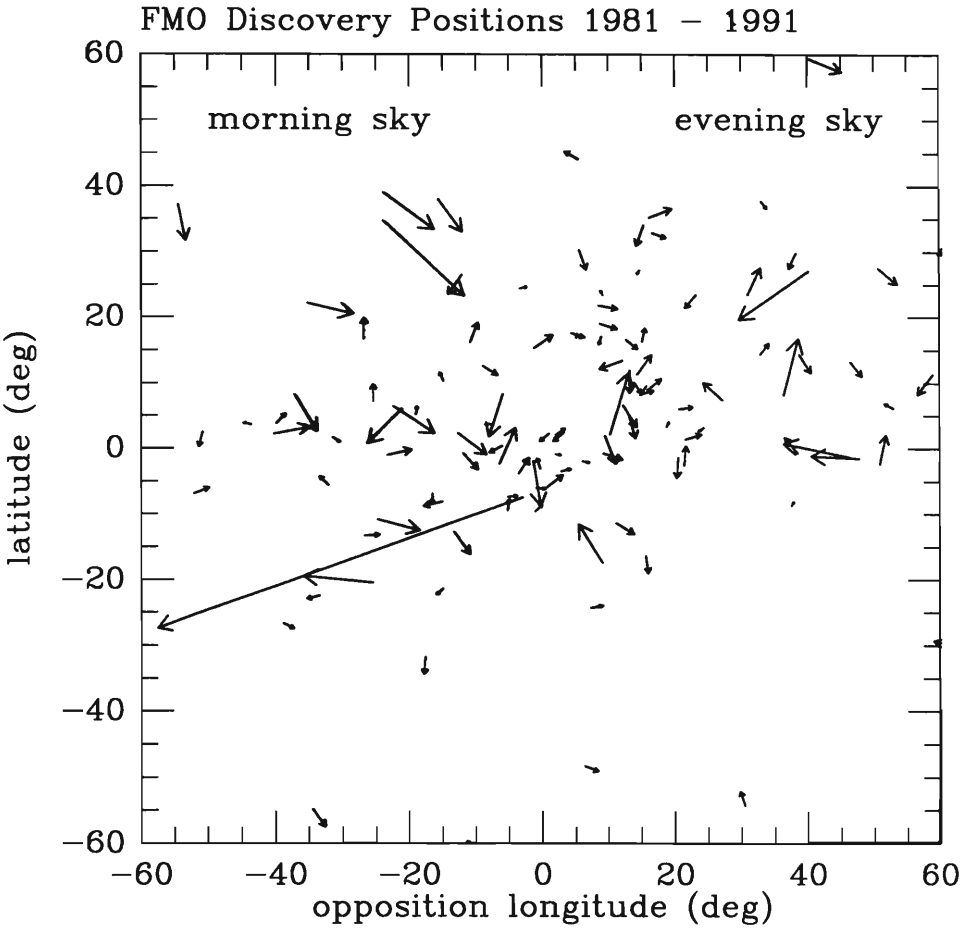

Figure 10. The discovery positions and angular velocities of NEAs discovered between 1981 and 1991. The longest velocity vector belongs to tiny 1991 BA, which was moving at about 1 arcsec per second at its discovery.

the dwell time as a measure of detectibility has to be modified by the angular velocity of the object with respect to any pre-set tracking rate. It is possible to use this angular velocity, or even simpler, direct or retrograde motion to help discriminate classes of NEAs. For example, if a uniform distribution of asteroids is assumed with $i = 0°$ and $0.6<a<4.0$ then of those asteroids observed to move in a prograde direction at opposition, 37% are Apollos, 55% are Amors, and 8% are Mars crossers.

Because many different distributions of orbital elements, sizes and reflectance properties can account for the observed distribution, it is not possible to derive a unique distribution from the observed set, because there are more variables than observed parameters. Furthermore, many of the relevant variables are not readily available, such as the total time a volume of space is searched to a given limiting magnitude, the results of negative searches, etc. However, it is possible to test models of orbital elements and size or reflective

TABLE I

Fraction of Orbital Period within 1.0 and 1.2 AU

		Eccentricity									
		0.0	0.1	0.2	0.3	0.4	0.5	0.6	0.7	0.8	0.9
	0.7	-	-	-	-	-	.254	.380	.466	.272	.211
	0.8	-	-	-	.239	.384	.471	.245	.189	.157	.135
	0.9	-	-	.365	.468	.276	.197	.157	.131	.113	.100
	1.0	1	.532	.564	.257	.184	.144	.119	.102	.089	.078
	1.1	1	.726	.300	.196	.146	.116	.097	.083	.072	.064
a	1.2	1	.463	.285	.171	.125	.099	.082	.070	.061	.054
(AU)	1.3	0	.195	.310	.166	.113	.087	.072	.061	.053	.047
	1.4	0	0	.197	.189	.107	.079	.064	.054	.046	.041
	1.5	0	0	0	.191	.107	.074	.058	.048	.041	.036
	1.6	0	0	0	.126	.117	.071	.054	.044	.037	.032
	1.7	0	0	0	.039	.145	.069	.050	.040	.034	.029
	1.8	0	0	0	0	.110	.071	.048	.037	.031	.027

property distributions against observations by holding at least one parameter constant. Such tests indicate that the assumption of a uniform distribution in a, e and i within their possible ranges, and an exponential distribution in absolute brightness (e^H) or a power-law distribution of diameter (d^k) leads to a good representation of the observed distribution of discovery parameters. However, because some volumes of parameter space have not been fully explored, (e.g., nearer the Sun, extremely small sizes, etc.), extrapolation to these regions is not necessarily warranted. In fact, recent discoveries by the Spacewatch Telescope suggest that there is an excess of small ($<$100 m) objects over an extrapolation from the power-law distribution observed with that telescope for larger NEAs (Rabinowitz 1992,1993).

No object is known to move permanently inside the orbit of the Earth. Making even a slight extrapolation from observed eccentricities and semimajor axes, however, indicates that such objects are to be expected. Furthermore, on dynamical grounds it is predicted that such orbits have been or will be achieved by a secular decrease of the eccentricities of Aten asteroids, or by a decrease of the semimajor axes of Apollos and Amors through close encounters with Mercury and Venus. An example of an infraterrestrial object is a fireball (no. 331) found by Halliday et al. (1989) to be moving in an orbit that just barely crosses the orbit of the Earth at its aphelion. Another hypothetical group of such objects are the vulcanoids, those interior to Mercury, left over from the formation of the planets. A search for these vulcanoids at thermal infrared wavelengths, and a compilation of previous searches in the vicinity of the Sun, is detailed by Leake et al. (1987). Other searches for faint objects close to the Sun during solar eclipses are described by von Klüber (1932) and Dossin (1966), while Kresak (1983) addresses their orbital stability. True vulcanoids, with orbits such that they can avoid being swept up or perturbed by Mercury, can best be detected at thermal wavelengths when the objects are at quadrature. Short of thermal wavelengths, infraterrestrial asteroids are at their brightest at superior conjuction, when the solar elongation is prohibitively small, but fade quickly as the elongation increases. Table II shows the brightness decrease or increase (negative values) of an asteroid with a Bowell-Lumme phase function of 0.25 as a function of four heliocentric distances and the Earth-Sun-asteroid angle (Bowell et al. 1989).

Recently a new survey at solar elongations between 28 and 40° was completed at the Llano del Hato Observatory of the Centro de Investigaciones de Astronomia near Merida, Venezuela by Hoffmann and Geyer. A 1 m Schmidt telescope was used each morning from January to March 1989 to obtain one plate per day (at best) for a given elongation, tracking at the sidereal rate. Although the results from this survey were negative, it can be used to set some upper limits to vulcanoid populations. Assuming a uniform distribution of orbital inclinations up to 60°, and a uniform distribution of the other orbital elements, 1.4% of such objects should have passed through the search fields during the survey. Taking the motion of the sky into account, the nondetection is equivalent to an upper limit of 240 objects with diameters of 6 km or greater,

TABLE II

Change in Apparent Magnitude as a Function of Heliocentric Distance (AU) and Earth-Sun-Asteroid Angle *C*

E-S-A Angle *C*	AU				E-S-A Angle *C*	AU			
	0.10	0.35	0.60	0.85		0.10	0.35	0.60	0.85
6	38.6	34.0	23.8	7.8	102	-6.0	-0.2	2.5	4.4
18	13.6	13.8	9.0	2.5	114	-6.8	-0.5	2.4	4.4
30	6.4	7.6	5.1	2.7	126	-7.4	-0.9	2.2	4.3
42	2.1	4.4	3.7	3.2	138	-8.0	-1.3	1.9	4.1
54	−0.8	2.6	3.1	3.7	150	-8.6	-1.7	1.6	3.9
66	−2.7	1.5	2.9	4.0	162	-9.3	-2.2	1.1	3.5
78	−4.1	0.8	2.7	4.2	174	-10.1	-3.0	0.5	2.9
90	−5.2	0.3	2.6	4.4					

or 75 objects with diameters of 10 km or more. No conclusion can be made for bodies with diameters of <5 km, or for populations always closer to the Sun than 28°, where searches are best conducted in the thermal infrared. Other previous and future surveys, systematic, casual, and during eclipses, that yield negative results should be analyzed and used to help sharpen the upper limits set here. Similar surveys taken from latitudes of about 50° on the Earth around the summer solistice, or from polar latitudes around the winter solistice, would take advantage of the prolonged twilight conditions that prevail as the Sun moves parallel to, but below the horizon. This condition allows protracted observational accessiblilty of objects at small elongations from the Sun.

III. SEARCH INSTRUMENTS AND TECHNIQUES

Summaries of current asteroid searches and their instrumentation and techniques are given by Helin and Dunbar (1990), Shoemaker et al. (1990), Gehrels (1991) and Rabinowitz (1991). The lion's share of discoveries of NEAs are credited to E. and C. Shoemaker and E. Helin. The method that has contributed the most discoveries in the past has relied on the use of the 0.46 m Schmidt on Palomar Mountain and the use of hyper-sensitized photographic plates. Two plates of the same field of view are taken about 45 minutes apart and visually compared with a stereo microscope. A moving object appears at a different depth than that of the fixed field stars if it has moved between exposures. NEAs are identified by their streaked shape or peculiar rate of motion relative to more distant moving objects. Recently, a new method of finding NEAs has come into play. At the Spacewatch Telescope of the University of Arizona at Kitt Peak, a TK2048 CCD is read out in drift-scan mode by a real-time computer system. The computer has been programmed to recognize trailed images and to detect moving objects by their change in position between three consecutive scans. This system is finding NEAs at a greater rate than any other method (15 objects in the first 10 months of regular operation) and is also extending the limits of detection. For the first time, asteroids smaller than 100 m are being found near the Earth, and larger NEAs are being found as far away as 2 AU.

Although the combined efforts of observers using Schmidt telescopes throughout the world has increased the rate of NEA discoveries in recent years, it is clear that the photographic method employed on these telescopes is reaching the limit of its capabilities. It is doubtful that emulsions with a quantum efficiency greater than 15% will ever be developed (K. Russell, personal communication). The potential of CCDs, on the other hand, is only just beginning to be explored. Quantum efficiencies as high as 80% are promised in the near future, and the CCDs will have greater resolution. A telescope designed to move rapidly across the sky, with the CCD read out at a high rate to match the motion of the sky across the field of view, could achieve the same area coverage as a Schmidt telescope without compromising its limiting magnitude for fast-moving objects. In principle, a marriage between CCD and

Schmidt telescopes could achieve the highest detection rate. Unfortunately, the difficulty of covering the large, curved field of view of a Schmidt with the small, flat areas of CCD chips would have to be solved. Current CCDs require an extensive housing for electrical connections and cooling with liquid nitrogen. It is doubtful that an array of CCDs could be built to take advantage of the wide field of the Schmidt unless the cooling requirement were eliminated, and the electrical connections reduced.

One other instrument that was successful at finding NEAs in the past was the Infrared Astronomical Satellite (IRAS). In the brief time it was operational (~8 months), it discovered two NEAs and one Earth-crossing comet (Green et al. 1985). These discoveries were made despite the fact that the satellite had not been designed to find NEAs. The area of the sky roughly 90° from opposition was scanned at intervals of roughly 100 min, but the overlap between consecutive scans was only 50%. As a result, there was a strong bias against multiple observations of retrograde NEAs. Also, some of the detector elements on the satellite were not functional. It is thus possible that the best instrument for detecting NEAs would not require high-resolution imaging at visual wavelengths. Instead, an infrared detector with low spatial resolution might accomplish the job more efficiently. For each NEA discovered by such an instrument, follow-up observations could be made with a CCD for confirmation and astrometry. The lesson to be learned here, however, is not that CCDs, or photographic plates, or infrared detectors offer the best solution. In the long run, the best method will be determined by whatever technology is currently available that can image a large area of the sky to faint limiting magnitudes without being swamped by detections of stars, galaxies, and other stationary objects. Perhaps a "smart" chip could be developed that would only respond to objects in motion, essentially an artificial retina.

IV. CONCLUSIONS

We have summarized in this chapter current strategies for finding near-Earth asteroids and have also suggested new ones. These strategies are appropriate given the distribution of orbits for the known NEAs. It is clear, however, that there are strong observational biases in this distribution. The NEA population is a highly structured complex. It has diverse origins, while Jupiter and the terrestrial planets have affected the distribution dynamically. The delivery process from the main belt to the Earth is particularly complex. The task of debiasing the observed distribution is therefore a formidable one. A physically plausible distribution must first be constructed and then tested by modeling the observational selection effects. If the predicted distribution matches the observed one, then the assumed distribution may be the true one, but not necessarily. While this task remains a challenge for the future, at least significant progress has been made in the development of search instruments and techniques. With the advent of CCD scanning, the current discovery rate of NEAs by observers world-wide has doubled. Improvements in the use of

CCDs within the next few years will double the discovery rate again. If the objective of these efforts is to detect all the NEAs in the solar system larger than a given size, however, the search must be directed in such a way as to minimize the observational biases. At the same time, our understanding of the physical processes that have created the NEA population must be used to guide the observations. Otherwise, it can never be known with certainty whether the near-Earth asteroids that are observed represent the complete population.

Acknowledgments. J. S. Lewis and T. Triffet are acknowledged for their continuing support of Spacewatch, and through SERC, for the support of J. D. while composing this chapter. Reviewer A. Milani and another anonomyous (but thorough) referee helped to improve the chapter, and E. Helin provided critical input.

REFERENCES

Bowell, E., Hapke, B., Domingue, D., Lumme, K., Peltoniemi, J., and Harris, A. 1989. Application of photometric models to asteroids. In *Asteroids II*, eds. R. P. Binzel, T. Gehrels and M. S. Matthews (Tucson: Univ. of Arizona Press), pp. 524–556.

Dossin, F. 1966. Comètes faibles au voisinage du soleil. *Mem. (8°) Soc. Roy. Sci. Liège* 5:12.

Drummond, J. D. 1991. Earth-approaching asteroid streams. *Icarus* 89:14–25.

Fernandez, J. A., and Ip, W.-H. 1991. Statistical and evolutionary aspects of cometary orbits. In *Comets in the Post-Halley Era,* vol. I, eds. R. L. Newburn, Jr., M. Neugebauer and J. Rahe (Dordrecht: Kluwer), pp. 487–535.

Gehrels, T. 1991. Scanning with charge-coupled devices. *Space Sci. Rev.* 58:347–375.

Gradie, J. C., Chapman, C. R., and Tedesco, E. F. 1989. Distribution of taxonomic classes and the compositional structure of the asteroid belt. In *Asteroids II*, eds. R. P. Binzel, T. Gehrels and M. S. Matthews (Tucson: Univ. of Arizona Press), pp. 316–335.

Green, S. F., Davies, J. K., Eaton, N., Stewart, B. C., and Meadows, A. J. 1985. The detection of fast-moving asteroids and comets by IRAS. *Icarus* 64:517–527.

Hahn, G. 1988. A Data Base of Observing Conditions for Aten-Apollo-Amor Objects During the 20th Century. Uppsala Astronomical Obs. Rept. No. 45.

Halliday, I., Griffin, A. A., and Blackwell, A. T. 1989. Detailed records of many unrecovered meteorites in western Canada for which further searches are recommended. *Roy. Astron. Soc. Canada* 83:49–80.

Halliday, I., Griffin, A. A., and Blackwell, A. T. 1990. Evidence for the existence of groups of meteorite-producing asteroidal fragments. *Meteoritics* 25:93–99.

Helin, E. F., and Dunbar, R. S. 1990. Search techniques for near-Earth asteroids. *Vistas in Astron.* 33:21–37.

Hughes, D. W. 1990. Dust coma onset at large heliocentric distances. In *Asteroids, Comets, and Meteors II*, eds. C.-I. Lagerkvist, H. Rickman, B. A. Lindblad and M. Lindgren (Uppsala: Uppsala Univ. Reprocentalen), pp. 327–342.

Kresak, L. 1983. Dynamical interrelations between the smaller bodies of the Solar System. *Highlights in Astron.* 6:377–390.

Lagerkvist, C.-I., and Magnusson, P. 1990. Analysis of lightcurves. II. Phase curves in a generalized HG-system. *Astron. Astrophys. Suppl.* 86:119–165.

Leake, M. A., Chapman, C. R., Weidenschilling, S. J., Davis, D. R., and Greenberg, R. 1987. The chronology of Mercury's geological and geophysical evolution: The vulcanoid hypothesis. *Icarus* 71:350–375.

Milani, A., Hahn, G., Carpino, M., and Nobili, A. M. 1989. Dynamics of planet-crossing asteroids: Classes of orbital behavior. Project SPACEGUARD. *Icarus* 78:212–269.

Rabinowitz, D. L. 1991. Detection of earth-approaching asteroids in near real time. *Astron. J.* 101:1518–1529.

Rabinowitz, D. L. 1992. The flux of small asteroids near the Earth. In *Asteroids, Comets, Meteors 1991*, eds. A. W. Harris and E. Bowell (Houston: Lunar and Planetary Inst.), pp. 481–485.

Rabinowitz, D. L. 1993. The size distribution of the Earth-approaching asteroids. *Astrophys. J.*, in press.

Shoemaker, E. M., Wolfe, R. F., and Shoemaker, C. S. 1990. Asteroid and comet flux in the neighborhood of Earth. In *Global Catastrophes in Earth History,* eds. V. L. Sharpton and P. D. Ward, Geological Soc. of America SP-247 (Boulder: Geological Soc. of America), pp. 155–170.

Tedesco, E. F. 1989. Asteroid magnitudes, UBV colors, and IRAS albedos and diameters. In *Asteroids II*, eds. R. P. Binzel, T. Gehrels and M. S. Matthews (Tucson: Univ. of Arizona Press), pp. 1090–1138.

Tedesco, E. F., Williams, J. G., Matson, D. L., Veeder, G. J., Gradie, G. J., and Lebofsky, L. A. 1989. A three-parameter asteroid taxonomy. *Astron. J.* 97:580–606.

von Klüber, H. 1932. Über Nachforschungen nach intramerkuriellen Körpern. *Astron. Nach.* 244:307–314.

Wetherill, G. W. 1991. End products of cometary evolution: Cometary origin of earth-crossing bodies of asteroidal parents. In *Comets in the Post-Halley Era*, vol. II, eds. R. L. Newburn, Jr., M. Neugebauer and J. Rahe (Dordrecht: Kluwer), pp. 537–556.